

An intermediate-scale model for thermal hydrology in low-relief permafrost-affected landscapes

Ahmad Jan^a, Ethan T. Coon^b, Scott L. Painter^a, Rao Garimella^c, J. David Moulton^c

^a*Climate Change Science Institute and Environmental Sciences Division, Oak Ridge National Laboratory, Oak Ridge, Tennessee, USA*

^b*Computational Earth Sciences Group, Earth and Environmental Sciences Division, Los Alamos National Laboratory, Los Alamos, New Mexico, USA*

^c*Applied Mathematics and Plasma Physics Group, Theoretical Division, Los Alamos National Laboratory, Los Alamos, New Mexico, USA*

Abstract

Integrated surface/subsurface models for simulating the thermal hydrology of permafrost-affected regions in a warming climate have recently become available, but computational demands of those new process-rich simulation tools have thus far limited their applications to one-dimensional or small two-dimensional simulations. We present a mixed-dimensional model structure for efficiently simulating surface/subsurface thermal hydrology in low-relief permafrost regions at watershed scales. The approach solves an operator-split system, sequentially coupling a two-dimensional surface thermal hydrology system with a family of one-dimensional vertical columns, where each column represents a fully coupled surface/subsurface thermal hydrology system without lateral flows. The overland thermal hydrology system with no sources acts to redistribute mass and energy horizontally by updating the column systems before they advance in time. We show that the approach is highly scalable, supports subcycling of different processes, and compares well with the corresponding

¹This manuscript has been authored by UT-Battelle, LLC under Contract No. DE-AC05-00OR22725 with the U.S. Department of Energy. The United States Government retains and the publisher, by accepting the article for publication, acknowledges that the United States Government retains a non-exclusive, paid-up, irrevocable, worldwide license to publish or reproduce the published form of this manuscript, or allow others to do so, for United States Government purposes. The Department of Energy will provide public access to these results of federally sponsored research in accordance with the DOE Public Access Plan (<http://energy.gov/downloads/doe-public-access-plan>)

fully three-dimensional representation at significantly less computational cost. These advances enable state-of-the-art representations of freezing soil physics to be coupled with thermal overland flow and surface energy balance at scales of 100s of meters. Although developed and demonstrated for permafrost thermal hydrology, the mixed-dimensional model structure is applicable to integrated surface/subsurface thermal hydrology in general.

Keywords: Mixed-dimensional model, Permafrost thermal hydrology, Integrated surface/subsurface flow modeling, Arctic

1. Introduction

Approximately 23% of the land surface in the Northern Hemisphere is underlain by continuous permafrost (91-100% frozen area), and another 17% is occupied by discontinuous permafrost (50-90% frozen area) [1, 2]. A massive
5 amount of organic carbon is stored in those regions [3, 4], which are warming at a rate considerably faster than the rest of the planet [5, 6, 7]. As the soils in that region warm, they have the potential to transform from a net sink to a net source of carbon to the atmosphere, which could increase the concentration of carbon in the atmosphere and in turn lead to further increase in the temperature (e.g.
10 [8]). Further, thawing and the resulting degradation of permafrost can cause significant changes in the surface and subsurface thermal hydrology and eventually can substantially alter the Arctic tundra ecosystems [9, 10, 11, 12, 13].

Those potential impacts and feedbacks in the terrestrial Arctic have motivated the development of increasingly sophisticated tools for simulating permafrost dynamics in a warming climate. Such simulations can help to better un-
15 derstand the consequences of soil warming and responses of tundra ecosystems to warming trends, and further expose the effects of permafrost degradation on surface and subsurface thermal hydrology. However, simulating permafrost dynamics in a complex and coupled surface/subsurface thermal hydrological environment is a challenging task, especially at larger spatiotemporal scales [14].
20 A comprehensive review of the modeling efforts of the surface and subsurface can

be found in [15]. Early research efforts focused on one-dimensional simulations for fundamental understanding of infiltration in cold climates; see, for example, [16, 17, 18]. Similar one-dimensional approximations have been adopted
25 as coarse-scale models in global land surface models [19, 20, 21, 13]. Two-dimensional simulations with simplified physics (i.e. saturated conditions, subsurface only) have been used for understanding evolution of field-scale groundwater systems [22, 23], but do not represent key unsaturated zone processes that are needed to understand active layer dynamics and decomposition of soil
30 organic matter. It is worth pointing out that mathematical models with limited complexity, reduced dimensionality, and relatively coarse spatial resolutions provide some insight into permafrost dynamics but fail to represent important processes such as cryosuction, lateral surface and subsurface flows, and advective heat transfers. Simulations with more mechanistic representations of surface and
35 vadose zone process in three-dimensions are essential to accurately capture the potential impacts of permafrost thawing on the surface and subsurface thermal hydrology and the resulting effects on the carbon cycle.

Two- and three-dimensional models with explicit physics-based representations of ice/liquid/gas partitioning in the vadose zone [24] have only recently
40 started to appear. Painter [2011] developed the three-phase, two-component model MarsFlo which has been used in Mars [26] and Earth permafrost studies [27]. Karra et al. [2014] simplified that subsurface freezing-soil thermal hydrology representation by ignoring gas advection and implemented that Richards-like approximation in the highly parallel PFLOTRAN [29] code. Kumar et
45 al. [2016] used that implementation in three-dimensional microtopography-resolving thermal hydrology simulations of polygonal tundra. Those computer codes are all subsurface-only models; that is, they do not represent surface flows and surface energy balance. Painter et al. 2016 recently introduced the Arctic Terrestrial Simulator, which uses a sophisticated multiphysics management frame-
50 work [32] to couple the three-dimensional subsurface representation of [28] with a two-dimensional non-isothermal surface flow model, surface energy balance with and without snow, and a simple snow distribution model.

Despite the significant progress in developing integrated surface/subsurface permafrost thermal hydrology models, significant challenges remain in moving
55 to climate-relevant spatiotemporal scales. One of the challenges is that the integrated system is numerically stiff because of the highly dynamic surface system [31] and the ice-liquid phase transition [33], which often results in relatively small time steps to achieve convergence. Small time steps are not problematic in one-dimensional simulations because a well-designed simulation tool will re-
60 cover the time step quickly after a convergence failure. However, a small time step becomes problematic in large three-dimensional runs because it becomes increasingly likely that, at any given time, at least one computational cell will be experiencing a phase change and thus a small time step. The other major challenge is tracking thaw-induced subsidence. Traditional hydrological simulators
65 are mainly designed to conduct three-dimensional simulations, however, deformations in a three-dimensional simulation are not easy to track due to mesh tangling and can be computationally expensive; further, poor mesh quality may raise questions about the accuracy of the results.

To address the aforementioned challenges, we present a mixed-dimensional
70 modeling strategy for process-rich simulations of integrated surface and subsurface thermal hydrology in tundra systems with low topographic gradients. The approach is intended for spatial scales intermediate between microtopography-resolving fine-scale simulations and the scale of an Earth system model grid cell. We demonstrate with simulations of polygonal tundra, large and carbon-rich re-
75 gions of northern Siberia, Alaska, and Canada where soil cracking has led to the formation of subsurface ice wedges that honeycomb the subsurface and tessellate the land surface into polygonal patterns. Rather than solve a fully three-dimensional subsurface system tightly coupled to surface processes as in [31], we take advantage of physical insights gained from fine-scale simulations and
80 approximate the integrated surface/subsurface dynamics with mutually independent 1-D columns, each associated with an ice wedge polygon. The columns are then sequentially coupled to a surface thermal flow system, solving the surface problem in an operator-split manner. This mixed-dimensional modeling

approach is motivated by fine-scale simulations at the ice-wedge polygon scale
85 that showed that differences in the thermal conditions among centers, rims and
troughs of ice-wedge polygons are largely equilibrated by lateral heat transport
during summer such that the system behaves similarly to a one-dimensional
system on seasonal time scales. Mixed-dimensional model structures have been
used previously in simulations of variably saturated flow at watershed scales,
90 in particular to couple multiple 1-D unsaturated (vadose) zone representations
to a two- or three-dimensional saturated zone; for example see [34, 35, 36].
Here we apply the mixed-dimensional model structure to an integrated sur-
face/subsurface flow system including surface and subsurface thermal processes
and evaluate the accuracy and computational advantages of the approximation.

95 The paper is organized as follows: Section 2 highlights the Advanced/Arctic
Terrestrial Simulator (ATS) and the Arcos multiphysics management frame-
work, within which we implemented our approach. Section 3 presents some
fine-scale simulation results and analysis that motivated the approach. In Sec-
tion 4 we introduce our mixed-dimensional modeling approach, loosely coupled
100 scheme and the ATS refactoring strategy. To illustrate the performance and ef-
ficiency of our modeling strategy, in Section 5 we compare our numerical results
with the three-dimensional simulations based on strong coupling, and present
speedup and scalability of the new technique. Concluding remarks and future
research are offered in Section 6.

105 2. The ATS Software

We implemented our mixed-dimensional modeling strategy in open-source
parallel software known as Amanzi-ATS [37] (or simply ATS). Amanzi-ATS is
the result of extending the flow and reactive transport simulator Amanzi [38]
by adding an advanced multiphysics management system known as Arcos [32].
110 Arcos is key to managing the complex spatial structures used here. It was
originally built to manage couplings among process models (denoted process
kernels and abbreviated as PKs), which may be selected at runtime. A PK

encapsulates the mathematical representation of a particular physical process or coupled set of processes; PKs are coupled together through Multiprocess
 115 Coordinators MPCs. An MPC is regarded as a PK by MPCs at higher levels in the tree, thus allowing complex hierarchical model structures to be built dynamically at runtime. In this work, we used Arcos to coordinate not only process kernels but also subdomains of the larger spatial domain.

Amanzi, and by extension ATS, uses the Trilinos [39] framework for parallel
 120 infrastructure. An unstructured mesh framework [40] is included for interacting with the computational mesh. General polyhedral meshes are supported. Discretization accuracy is maintained on the potentially distorted grids through the use of the mimetic finite difference (MFD) method [41, 42]. The backward Euler method is used for time stepping with a Nonlinear Krylov Acceleration
 125 (NKA) method [43, 44] to solve the resulting discretized residual equations.

The initialism ATS may refer to either the Advanced Terrestrial Simulator, which is the general capability, or the Arctic Terrestrial Simulator, which is one particular configuration [31], depending on context. The Arctic Terrestrial Simulator configuration solves strongly coupled surface energy balance, and sur-
 130 face and subsurface thermal hydrology with freeze/thaw dynamics. This work extends the ATS to work with a multicolumn spatial structure.

3. Motivation: Results from Fine-scale Simulations

This mixed-dimensional approach is motivated by the results of fine-scale, two-dimensional simulations on vertical cross-sections across ice-wedge polygons
 135 at the Barrow Environmental Observatory. The simulations coupled a surface energy balance model with and without snow, snow distribution models, models for thermal overland flow including phase change, and a recently developed three-phase subsurface thermal hydrology model. The soil properties were calibrated against borehole temperature data in a previous study [45]. The simula-
 140 tions were forced with meteorological data for the site. Those simulations used an unstructured mesh that conforms to surface topography derived from lidar

measurements. Horizontal mesh resolution is approximately 0.25 m. Vertical resolution is 0.02 cm at the surface and gradually increases with depth. Details on boundary conditions and the spinup process can be found in [31].

145 Snapshots of ice and liquid saturation indices in cross-section across two ice-wedge polygons are shown in Fig. 1. These snapshots are for October 15, 2013, which is during the fall freeze-up. During this period, the rims of the ice-wedge polygons are significantly colder than the centers and troughs because the thermally insulating snowpack is smaller on the rims. Previous one-dimensional
150 simulations [46] have shown that thermal differences caused by differences in snow depth lead to differences in active layer thickness, the depth of the annual thaw. However, in the two-dimensional simulations shown here, the active layer thickness shows little variation across the polygon (Fig. 2). Although transient differences in subsurface temperature occur due to differences in snow depth, soil
155 moisture content, and albedo, lateral heat transport is sufficient to equilibrate those differences by the time of maximum thaw. Thus, the active layer thickness, which is a primary control on the annual carbon decomposition rates, is not directly affected by microtopographic position within an ice-wedge polygon in cases where organic matter is relatively uniform. This lack of sensitivity suggests
160 a model structure where the ice-wedge polygon becomes the unit computational cell on the surface.

4. An Intermediate-scale Model

Our intermediate-scale model has two components: a spatial structure that combines one-dimensional and two-dimensional domains, and an operator splitting
165 scheme for coupling. We describe those aspects in this section followed by the refactoring strategy of the ATS.

4.1. Mixed-Dimensional Modeling Approach

Our modeling strategy splits a 3D domain into $2N + 1$ subdomains, where N is the total number of surface elements. The workflow starts with a two-
170 dimensional tessellation of the land surface, where each polygon in the surface

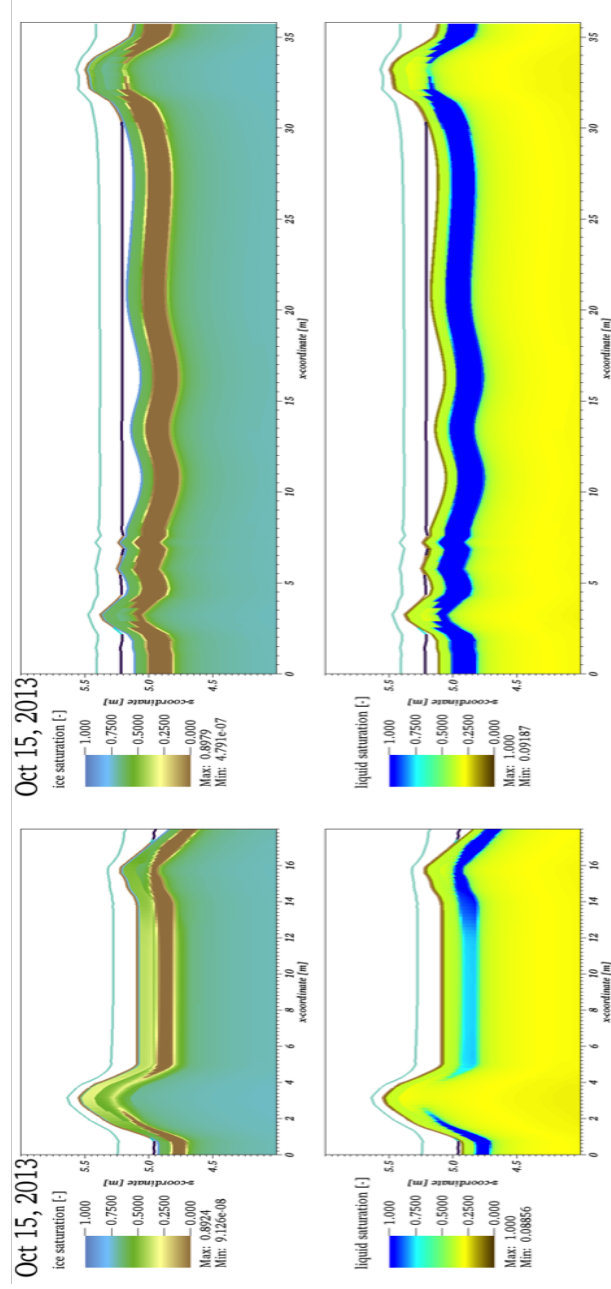


Figure 1: Results from two-dimensional fine-scale modeling. Shown are snapshots of ice saturation index and liquid saturation index in cross-sections across two ice-wedge polygons.

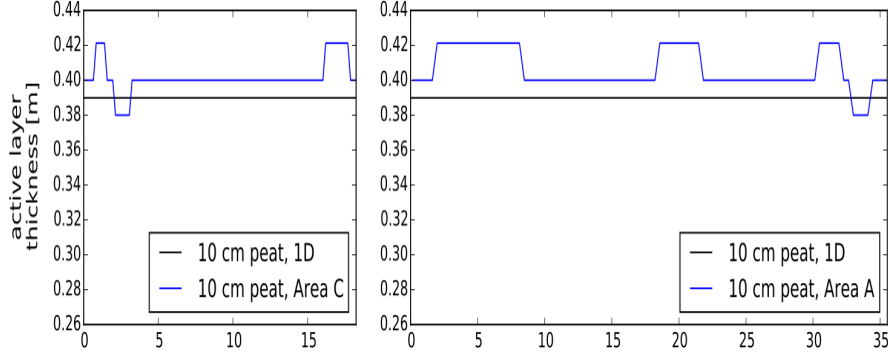


Figure 2: Active layer thickness from fine-scale modeling. Note that the mesh resolution here is 2cm , and the discontinuities reflect jumps between cells of the mesh.

mesh corresponds to an ice-wedge polygon. Standard mesh generation tools are then used to construct a 3D mesh by extruding each of the surface polygons vertically into the subsurface. This 3D mesh represents the entire domain of interest and is referred to as the primary mesh. Within ATS, the 3D primary mesh is then subdivided into $2N + 1$ submeshes, where N is the total number of surface elements. The total $2N + 1$ subdomains include N subdomains for 1D subsurface columns (on which flow and energy equations are solved), N subdomains as the surface of those columns (on which surface water and energy storage is tracked along with a surface energy balance calculation), and one subdomain for the 2D overland system, on which lateral surface flow is solved. To avoid confusion, hereafter the 2D overland flow system is referred to as an overland system, and the surface cell of each 1D columns will be called a column-surface system. The 1D columns and overland system are highlighted in Fig. 3. Arcos represents physics on these domains as a hierarchical PK tree which shows how the processes are coupled on and across these domains, as illustrated in Fig. 4. The PK tree consists of individual conservation equations, strong (globally implicit) couplers, and weak (sequential) couplers highlighted in blue, light cyan, and orange colors, respectively. In our approach, the interaction at the interface between the overland and 1D columns happens at

190 the top level weak MPC. The strong MPC (on the left at the second level) is
 the overland system. The weak MPC at the second level iterates over all the
 column subdomains. The PK-I, $I = 1, 2, 3, \dots, N$ denote an integrated system
 composed of surface energy balance, column-surface (a cell) and subsurface (1D
 column) system. The tree attached to the black octagon shape is replicated
 195 across all PK-I, $I = 1, 2, 3, \dots, N$.

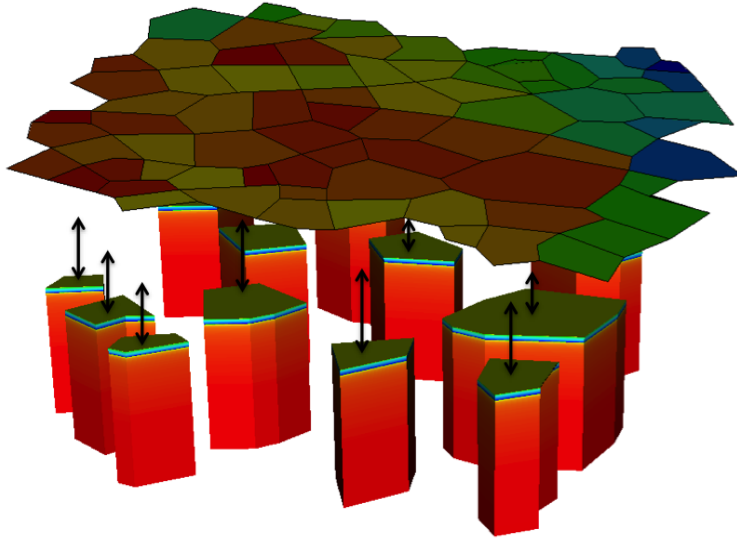


Figure 3: An illustration of the independent 1D subsurface columns coupled to the overland
 system. The column-surface system (1D cells lying on the top of corresponding columns) are
 not shown.

4.2. *Operator Splitting Scheme*

The operator splitting scheme for advancing our mixed-dimensional model
 is a two-step sequential algorithm. First, we solve the overland-flow thermal
 hydrology system without any external or exchanged sources and then compute
 200 the solution of the one-dimensional columns. Each 1D column is a system of
 the subsurface thermal hydrology, surface energy balance, and surface ponding
 and energy exchange with no lateral flow. The first step mainly acts as a spatial
 distributor of the mass and energy. That is, it distributes the water and energy

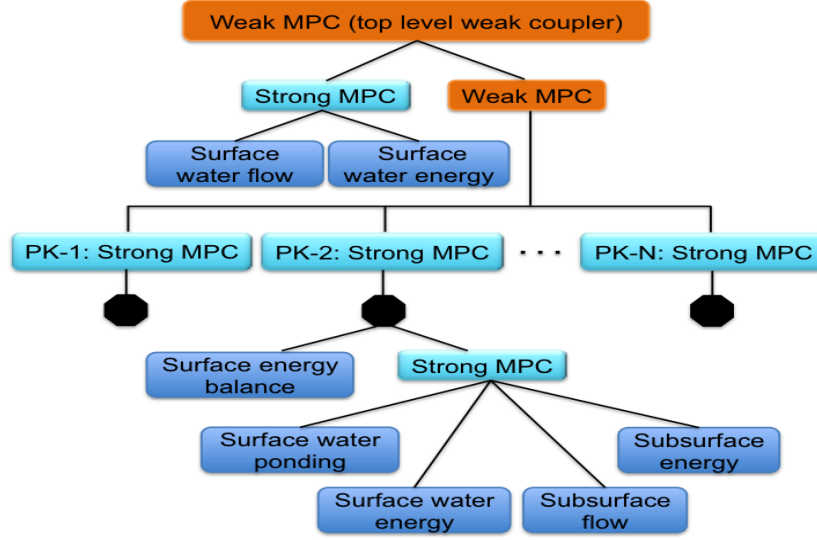


Figure 4: A customized hierarchical structure of the process kernels. Blue blocks highlights independent process models; Light blue blocks strongly coupled independent process kernels; Orange blocks represent weak couplers.

across the 2D overland system, and its solution serves as initial condition for
 205 the second step. After the update from the first step, we solve the family of
 1D columns, and use the output of that half-step to update the overland-flow
 pressure and temperature for the next iteration in the algorithm. As depicted in
 Fig. 5, the top and bottom orange spots represent 2D overland-flow system and
 1D columns, respectively, and the cyan colors (in the middle) are intermediate
 210 steps for updating overland-flow and 1D column systems. For the sake of clarity,
 we will refer to the pressure and temperature fields of the first step as overland-
 flow pressure and temperature, while that of the second step will be called as
 subsurface and column-surface pressures and temperatures.

4.3. ATS Refactoring Strategy

215 The ATS was significantly refactored to accommodate the above customized
 scheme. Arcos's state object stores a dynamic, runtime-determined set of sim-
 ulation data. Each data is identified by a unique key, e.g. "ponded_depth",

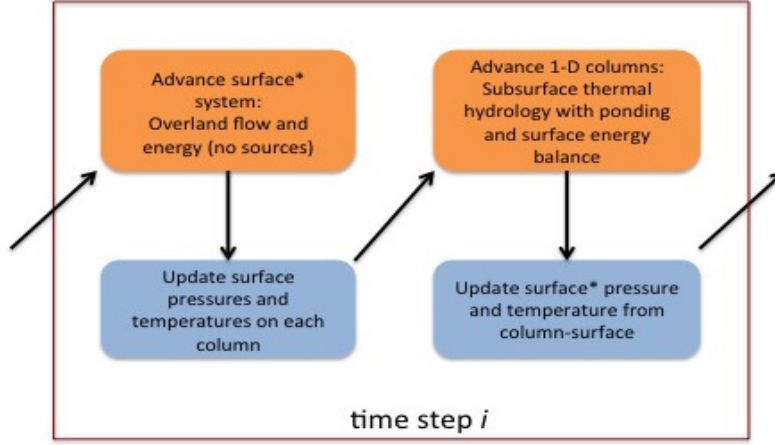


Figure 5: Schematic of the loosely coupled scheme for our mixed-dimensional model. Orange represents advancement of PKs in time; blue shows intermediate steps for initialization of PKs within a single time step.

and a set of metadata including domain of applicability, mesh entity, number of degrees of freedom, etc. In order for each PK to be instantiated multiple times, that PK’s data was altered to enforce uniqueness of its keys by prefixing a domain identifier such as “column_0_surface-ponded_depth”. This refactoring allows multiple instances of any given PK, each attached to a different mesh representing a subdomain of the primary mesh.

Furthermore, Amanzi-ATS relies on a meshing infrastructure, MSTK, [40] which can generate meshes as subdomains or subsets of existing meshes. This framework was extended to allow column meshes to be generated from an existing three-dimensional mesh. In this workflow, a surface mesh consisting of the surface polygons are extruded vertically, following pre-determined soil horizon structure, to create a 3D mesh. By insisting that the extrusion process works only in the vertical, well-defined columns then exist in the the three-dimensional mesh. At run-time, columns can then be identified, and extracted to form a one-dimensional mesh. This mesh is altered to ensure it is a one-dimensional submanifold of three-dimensional space, i.e. each cell has two faces, and all

face-normals are $\pm\hat{z}$. Once this is done, Amanzi-ATS’s existing operators can
 235 work on this mesh without changes. Furthermore, this mesh follows polygonal
 ground, and therefore consists of stacked polygonal-prisms. Few mesh capabilities
 support this fully-unstructured mesh type; a Silo[47] capability was added to
 to Amanzi-ATS’s existing output options to enable visualization of the resulting
 solution.

240 Each of these refactors was accomplished in reasonable time thanks to a
 close adherence to computational software best practices. A series of unit and
 regression tests were added for each new capability, and the existing regression
 tests were updated with the domain prefixes. Version control enabled close col-
 laboration on this process across multiple developers, and project-management
 245 Kanban tools were used to ensure each developer in the workflow knew the
 needs of the client code component. These best practices, along with the use
 of libraries such as Silo, MSTK, and Arcos, greatly improved the efficiency of
 what otherwise would have been a significant development effort.

5. Results and Discussions

250 In this section, we present numerical results that highlights the accuracy and
 efficiency of our modeling technique. At the development stage, several numeri-
 cal experiments were performed to verify the physical behavior of the refactored
 modules (PKs) of the ATS, code verification details are presented in Appendix
 A. The spinup process (i.e., model’s initialization) has been described in detail
 255 in [31].

5.1. Numerical Results – A Comparative Study

To demonstrate the accuracy of our modeling technique, we compare nu-
 merical results of the mixed-dimensional model against a fully coupled three-
 dimensional simulations that act as a benchmark for our simulations. The do-
 260 main under consideration has surface elevation varying between 4.14-4.62 m,
 is 40 m deep, and enclosed by a rectangle in the horizontal plane 173×160

m²; see Fig. 6. This domain is a part of the low-gradient polygonal tundra in Barrow, Alaska and consist of 75 ice wedge polygons. As highlighted in Fig. 6, we select five spots (based on different elevations) to perform a location-based comparison of the numerical results of the two schemes.

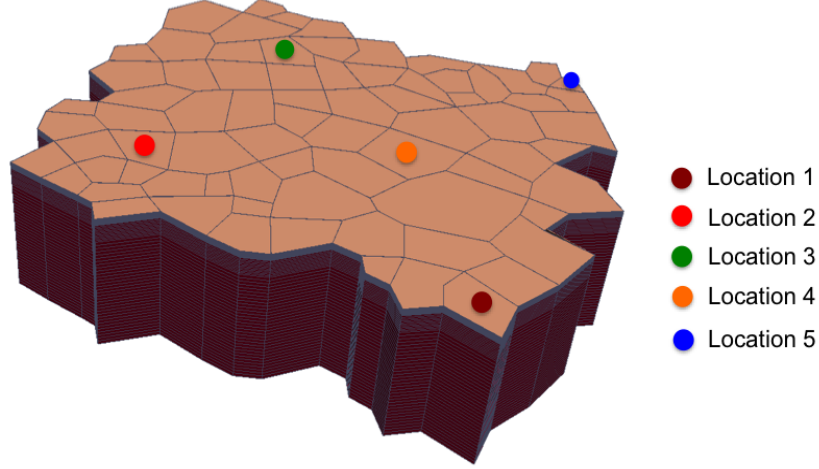


Figure 6: An illustration of the five spatial locations on 75 polygons cluster for location-based comparison of the two schemes. Location 1: Outlet. Location 2: High elevated spot. Location 3-4: Intermediate elevation spots. Location 5: Lowest elevation spot.

265

In addition to evaluating the quality of our mixed-dimensional approach for the Barrow tundra, we also want to understand when it will give inaccurate results. Because our modeling strategy is based on a loosely coupled scheme and neglects subsurface lateral flow between ice wedge polygons, it should eventually become inaccurate if the topographic relief is sufficiently large. To identify the range of applicability, we consider three variants of the surface topography. We use the following equation to exaggerate the surface topography,

$$\bar{Z} = \alpha(Z - \mu) + \mu. \quad (1)$$

Here \bar{Z} is the exaggerated elevation, Z is the original elevation with mean μ , and α is the exaggeration parameter. Equation (1) preserves the mean while the standard deviation depends on the value of α and is given in meters by 0.14α .

The coefficient in front of α is the standard deviation of the original elevation Z
 – in our case Z correspond to the domain shown in Fig. 6. Our three variants
 correspond to $\alpha = 1, 3$, and 5. The value $\alpha = 1$ corresponds to the original
 topography. We expect the model to give promising results for simulating low-
 gradient polygonal tundra, and believe that the values of α we choose provide
 sufficient variation across a domain of 100s of meter. Our numerical experiments
 confirm a high agreement between the results of the mixed-dimensional model
 and the 3D model at all selected location for all three α values. Figs. 7 and 8
 compare the subsurface water saturations and temperatures, respectively, at
 locations 1 and 5 and for $\alpha = 1$. The accuracy of our results for the Barrow
 topography ($\alpha = 1$) is evident. The surface ponded depths and temperatures
 obtained with the two models are depicted in Fig. 9 and 10, respectively. As
 expect, our results fit the 3D model’s results very well. We see the same level
 of agreement at the other locations as well, but we are not showing them here.
 In Fig. 11 we plot the mean annual thaw depth at five locations for the three
 variants, $\alpha = 1, 3$, and 5. We use the annual mean of the thaw depth rather
 than the maximum thaw depth (i.e. the active layer thickness) because the
 mean annual thaw depth depends on both the duration of thaw and maximum
 thaw depth. Thus it is a direct measure of soil available for decomposition,
 averaged over the year. Not surprisingly, as the value of α increases the mean
 annual thaw depth deviates from the results of the 3D model to some extent,
 but we still see the results of the mixed-dimensional model agree well with
 to the corresponding benchmark solution. The consistency of our numerical
 results with the fully coupled 3D simulations confirm the appropriateness of
 this approximated scheme.

5.2. Speedup Study

We discuss speedup and parallel efficiency for two spatial domains, one with
 75 polygons as depicted in Fig. 6 and a larger one consisting of 468 ice-wedge
 polygons, as shown in Fig 12. The surface ponded depth and temperature during
 the snowmelt in 2012 are presented in Fig. 13 for the 468 polygon domain. Fully

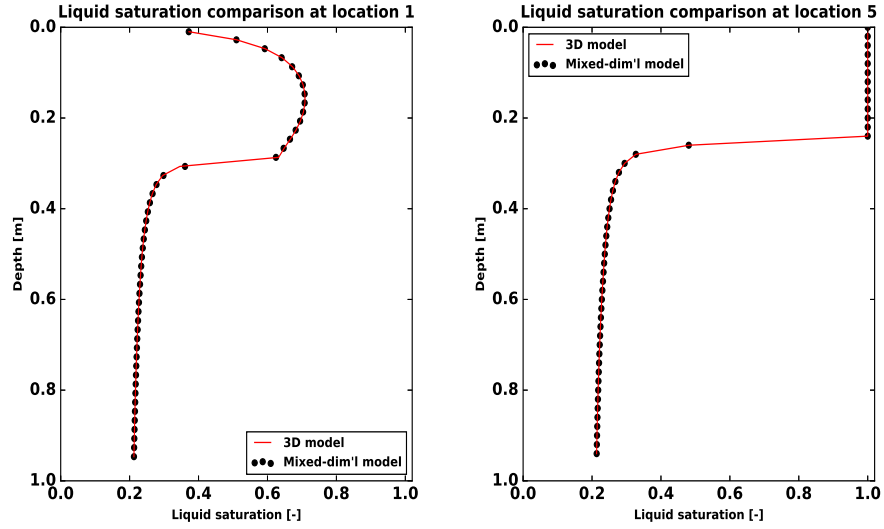


Figure 7: Comparison of the subsurface water saturation at locations 1 and 5 during the summer.

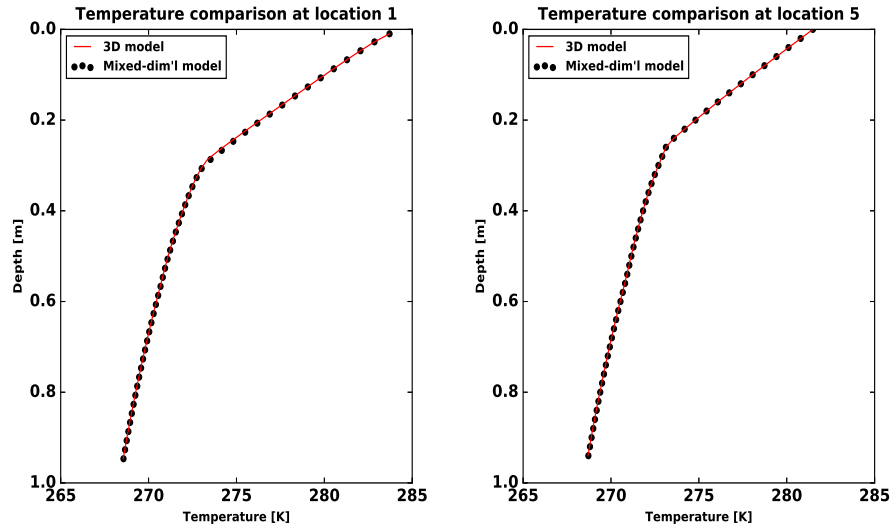


Figure 8: Comparison of subsurface temperature at locations 1 and 5 during the summer.

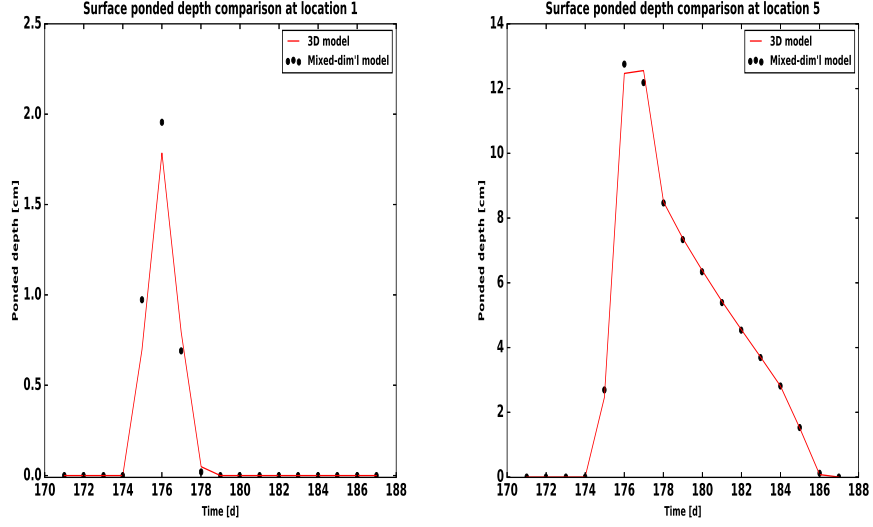


Figure 9: An illustration of the surface ponded depths of the two schemes at locations 1 and 5 when the snow melt starts.

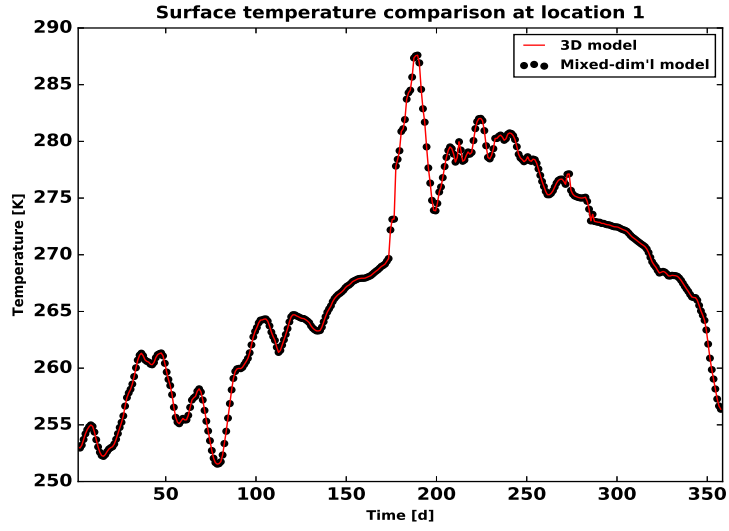


Figure 10: An illustration of the surface temperature of the two schemes at location 1 for the entire year.

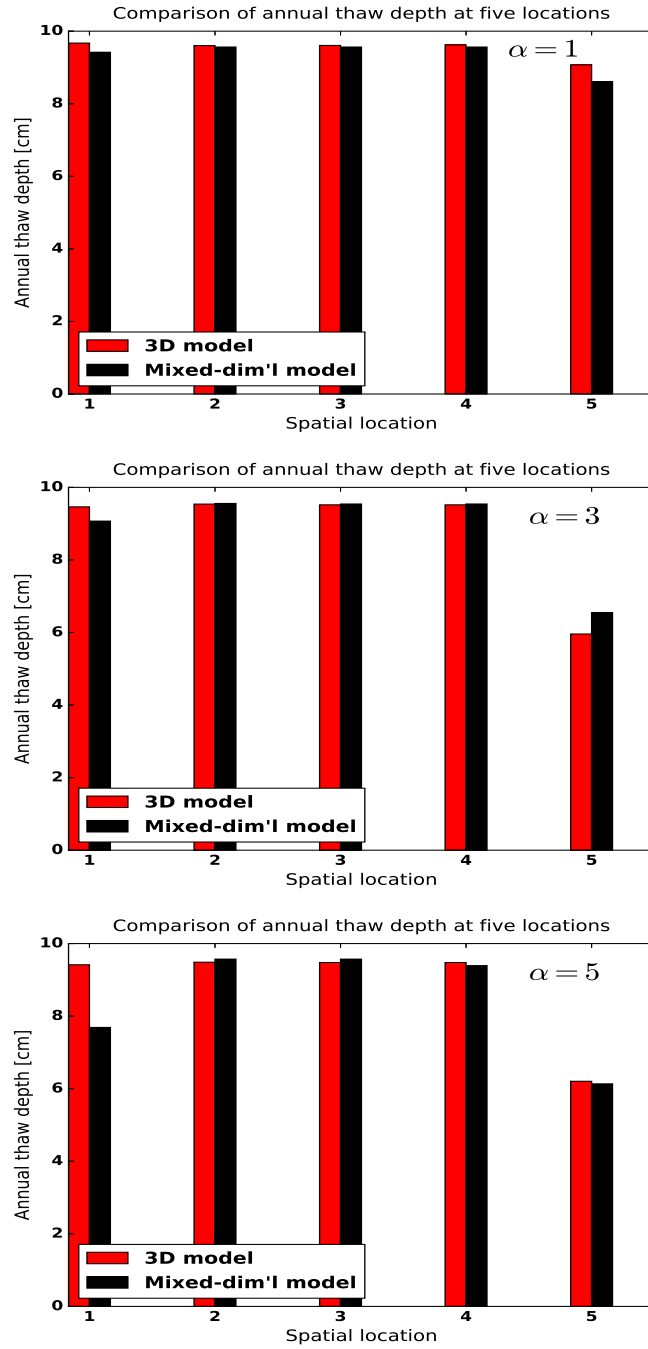


Figure 11: A comparison of the annual thaw depth at the selected locations of the three studies.

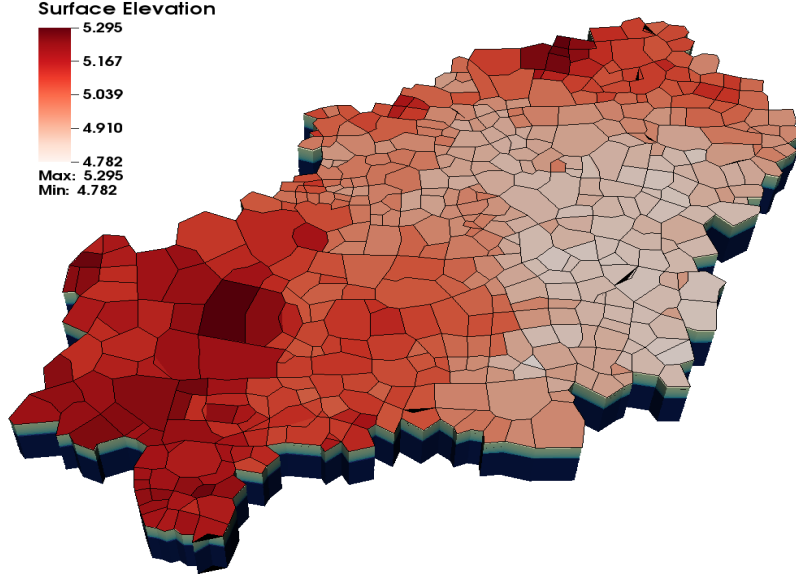


Figure 12: A watershed at Barrow, Alaska.

coupled 3D simulations at such a scale are computationally very expensive.

300 We highlight two aspects of the efficiency of this modeling approach: (i) how the simulation time decreases in comparison with three-dimensional simulations, and (ii) how efficiently it scales with number of processes.

Fig. 14 compares the computational time of the multidimensional strategy versus the three-dimensional solution for the domain consisting of 75 columns. 305 It can be seen that for a fixed number of processors, the computational time decreases by a factor of about four with the multidimensional technique. This is a huge computational advantage without sacrificing numerical accuracy.

We show parallel strong scaling for the aforementioned domains in Fig. 15. Speedup of the smaller domain is significantly less than the linear ideal; this 310 is caused by communication overhead in the overland-flow system. Without consideration of the overland-flow system, the problem is perfectly parallel. To minimize communication between the overland-flow system and the column systems, the overland-flow mesh is partitioned so that a column and the coincident

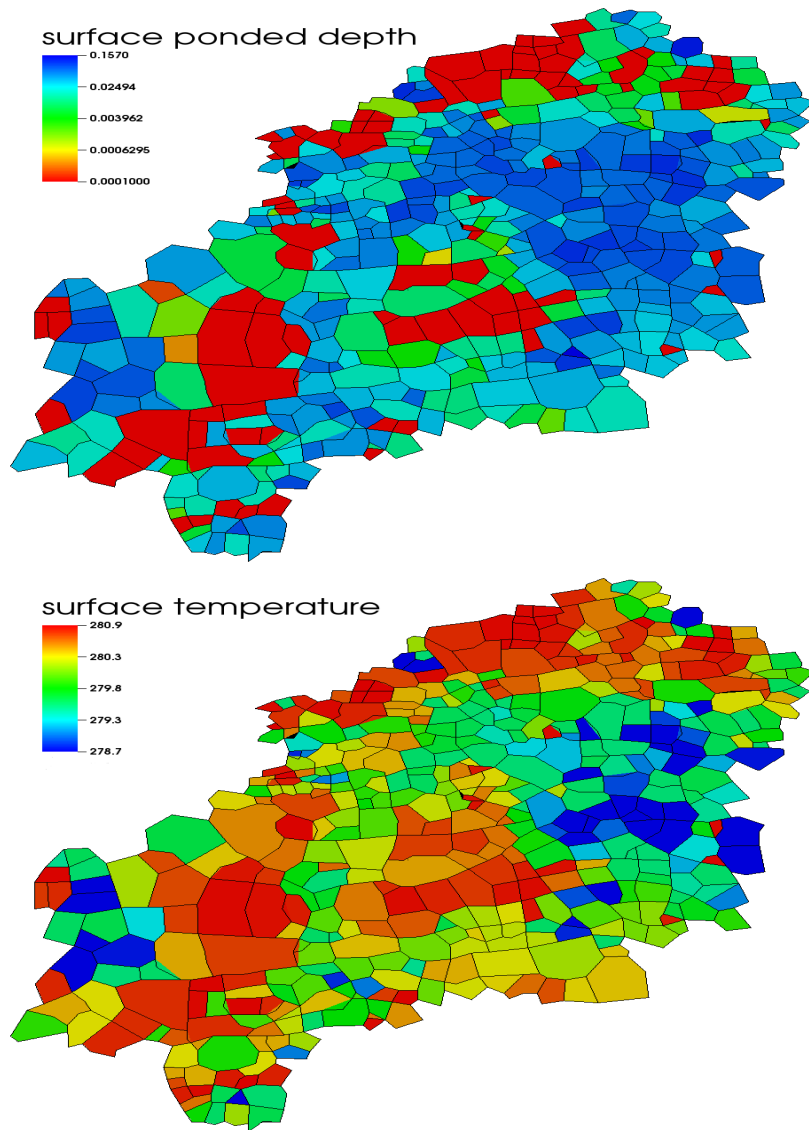


Figure 13: Simulation results of the mixed-dimensional model. Showing the surface ponded depth and temperature during the snowmelt of 2012.

mesh cells on the overland-flow system reside on the same processor. If there
 315 are too few columns per processor, the interprocessor communication for the
 overland-flow system becomes the limiting factor despite the lower computa-
 tional burden for the overland-flow system compared with the columns. As
 expected, the scaling is better for a larger domain. Scaling is close to linear up
 to about 16 cores, which corresponds to about 30 columns per core.

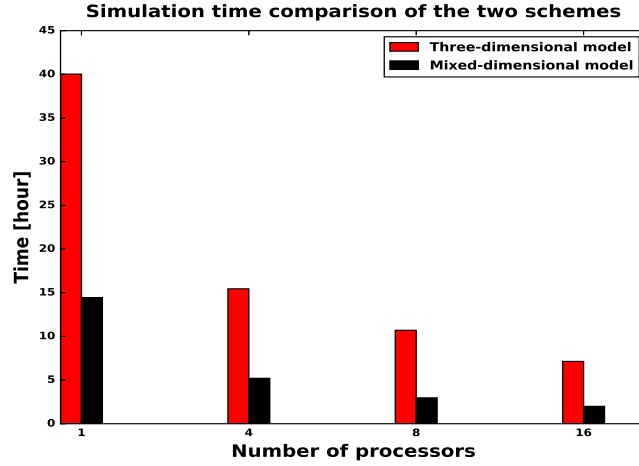


Figure 14: A comparison of the computational time taken by the mixed-dimensional and 3D models.

320 5.3. Subcycling Process Kernels

One advantage of sequentially coupling different PKs, as opposed to a fully
 coupled approach, is that sequential coupling makes subcycling possible. With
 subcycling, individual PKs take their own time step rather than a global time
 step. The independently evolving PKs are then synchronized on a larger time
 325 step. The idea is to assign a suitable local time-step to each subdomain rather
 than one single global time-step. It is a very convenient approach for simulating
 permafrost type regions because a relatively small time step may be required
 when a cell is going through a phase change. Without subcycling, a timestep
 failure or small timestep caused by phase change in a single cell results in a

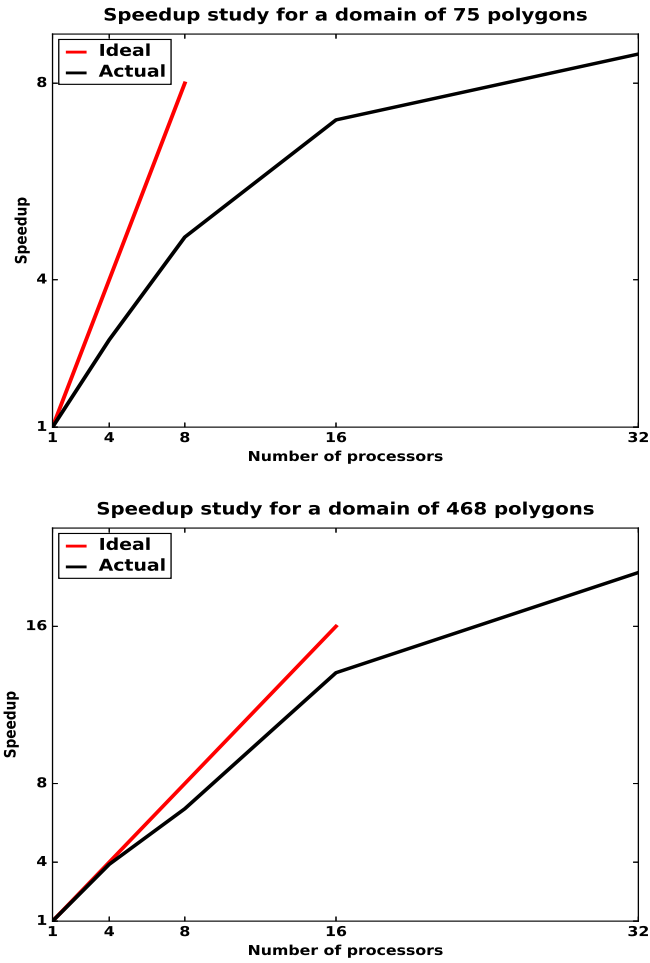


Figure 15: An illustration of the speedup study of a simulation with 75-polygon cluster (top) and 468 polygons barrow watershed (bottom).

330 small global time step. With subcycling, the effects of that phase transition
 are limited to a single column. Our mixed-dimensional modeling approach effi-
 ciently allows subcycling PKs because we discretize subsurface as independent
 columns/subdomains. Thus, the subdomains can advance in time with their
 preferred time-steps until they hit the synchronized time. Fig. 16 displays per-
 335 centage reduction in the simulation time for the domains consisting of 21, 75,
 and 468 polygons. With the increase in the number of subsurface columns the
 computational time decreases, and we see up to 40% reduction in the compu-
 tational time in comparison with simulations without subcycling. The choice
 of the synchronization time is crucial, and requires further optimization, which
 340 will be studied in future work.

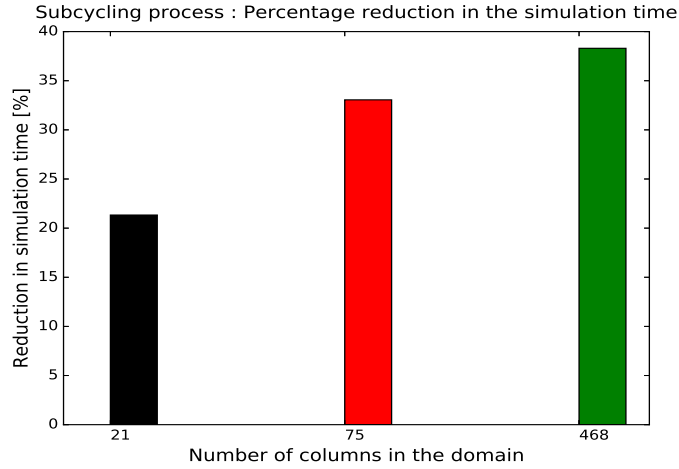


Figure 16: (Subcycling PKs) Percentage reduction in the computational time for the domains consisting of 21, 75 and 468 polygons.

6. Conclusions and Future Work

Our intermediate-scale model for integrated surface/subsurface thermal hydrology of low-relief permafrost-affected regions is constructed from two components: a mixed-dimensional spatial structure that is based on discretizing the

345 subsurface as independent columns that are indirectly coupled through a two-
dimensional surface system, and an operator splitting scheme for coupling the
column domains to the surface system. The spatial structure was motivated by
fine-scale simulations of permafrost regions. This is the first demonstration of
advanced representations of freezing soil physics coupled to overland thermal
350 flow and surface energy balance at scales of 100s of meters.

An operator splitting algorithm is used to advance our mixed-dimensional
model. First, we solve a two-dimensional surface thermal hydrology system that
spatially distributes mass and energy, and initializes the system of the second
step. The second step solves a family of independent one-dimensional columns,
355 where each represents an integrated system of the subsurface, surface ponding
and surface energy balance. That step updates the 2D surface system of the
first step for the next iteration.

We compared our numerical results to the conventional scheme of a fully 3D
subsurface that is strongly coupled to a surface system to demonstrate the effi-
360 ciency and accuracy of our modeling approach. The fully coupled results act as
a benchmark for our scheme. Numerical results show our scheme closely approx-
imates the fully coupled system but is significantly more efficient. The scheme
also allows for subcycling of individual subdomains, which further improves the
numerical efficiency.

365 This work is part of a larger effort to provide process-rich, watershed-scale
simulations capability for permafrost regions. A next step would be to incorpo-
rate a subgrid model to represent the effects of variations of topography below
our discretization unit of the ice wedge polygon. Another future direction is
to represent thaw-induced subsidence. Thawing of permafrost and melting of
370 massive subsurface ice can cause differential subsidence, leading to dynamic
microtopography (low-centered polygons can transform to high-centered poly-
gons) [48, 49], substantial changes in hydrology and soil moisture, and altered
drainage networks, thus potentially transforming a dry region to a wetland
ecosystem [50, 51]. This modeling strategy is designed to tractably represent
375 thaw-induced subsidence. Representing subsidence in one dimension is signif-

icantly easier than a fully three-dimensional representation because mesh tan-
gling and other mesh quality issues arise in a fully three-dimensional dynamic
mesh but are avoided in one dimension. Indeed, simulations of thaw-induced
subsidence on a single one-dimensional integrated surface/subsurface system has
380 already been demonstrated [14]; the work described here will allow the same
techniques to be used at scale with many columns coupled to an overland flow
system. Lastly, refactoring ATS not only supports subdomain modeling tech-
niques but is also potentially useful future extensions. We can efficiently imple-
ment and independently test many process representations (physical, chemical,
385 biological and geological processes) as PKs and let them interact through MPCs.

Although we mainly focus on simulating the thermal hydrology of degrad-
ing permafrost, elements of the work presented here have greater applicability.
A hybrid spatial structure mixing one-dimensional representations of the va-
dose zone with two-dimensional representations of the saturated zone and over-
390 land flow system are important approximations in watershed modeling. This
operator-split scheme of Fig. 5 is broadly applicable to those systems and to
integrated surface/subsurface simulations, in general. This mixed-dimensional
representation may be used as an alternative to a fully coupled system or as a
way of accelerating the time-consuming task of spinup. In addition, this work
395 demonstrates the advantages of Arcos or other multiphysics management frame-
works in greatly simplifies the process of building models with hybrid spatial
structure.

Acknowledgments

This work was supported by Interoperable Design of Extreme-scale Appli-
400 cation Software (IDEAS) project and by the Next Generation Ecosystem Ex-
periment (NGEE-Arctic) project. NGEE-Arctic is supported by the Office of
Biological and Environmental Research in the DOE Office of Science. We are
also grateful to Jitu Kumar, Lauren Charsley-Groffman, Terry Miller, Garrett
Altman and Lucia Short for help in constructing computational meshes.

405 **Appendix A. Numerical Experiments – Code Verification**

We have performed a series of tests at the development stage for code verification, and compared our results against numerical solution of three-dimensional model. The 3D results serve as a benchmark for our scheme. In 3D models the surface and subsurface systems are strongly coupled and solved implicitly. 410 Since our model required major refactoring of the ATS, so individual pieces of the code were deeply tested before integration – they are listed below:

- Problem Test 1 (Subsurface Flow): We consider multiple subsurface columns with flat top surface – each column is an independent domain. Put water table below the surface, infiltrates and fills the subsurface columns.
- 415 • Problem Test 2 (Surface and Subsurface Flow only): This is an extension of the Test 1. We put water table below the surface. Water infiltrates and fill subsurface columns prior to surface ponding.
- Problem Test 3 (Subsurface Thermal Hydrology): We add energy equation to Test 1. Initially, establish water table close to the surface, and start 420 freezing from below. The frozen subsurface columns are thawed from the top.
- Problem Test 4 (Surface and Subsurface Thermal Hydrology): In this test, we incorporate surface thermal hydrology into Test 3. A warm rain precipitation thaws the subsurface columns, saturate them and afterwards 425 water ponds on the surface.
- Problem Test 5 (Surface Energy Balance, Surface and Subsurface Thermal Hydrology): A fully integrated surface and subsurface processes test. We introduce an energy balance equation to Test 4. An initially established ice table below the surface has been thawed by warm rain, incoming-short 430 radiation and air temperature.

Due to symmetry in the domains of above numerical tests, that is, the subsurface columns are copies of each other and surface is flat, we get identical results

and compare very well with its corresponding three-dimensional simulation results. Passing all the above tests conclude refactoring of the ATS a success. In
435 the preceding discussion, we consider general polyhedra due to the polygonal structure of the Arctic landscape.

References

- [1] J. Brown, O. Ferrians Jr, J. Heginbottom, E. Melnikov, Circum-Arctic map of permafrost and ground-ice conditions, 45, 1997.
- 440 [2] M. T. Jorgenson, C. H. Racine, J. C. Walters, T. E. Osterkamp, Permafrost degradation and ecological changes associated with a warming climate in central alaska, Climatic change 48 (2001) 551–579.
- [3] E. A. G. Schuur, A. D. McGuire, C. Schaedel, G. Grosse, J. W. Harden, D. J. Hayes, G. Hugelius, C. D. Koven, P. Kuhry, D. M. Lawrence, S. M.
445 Natali, D. Olefeldt, V. E. Romanovsky, K. Schaefer, M. R. Turetsky, C. C. Treat, J. E. Vonk, Climate change and the permafrost carbon feedback, NATURE 520 (2015) 171–179.
- [4] G. Hugelius, J. Strauss, S. Zubrzycki, J. W. Harden, E. A. G. Schuur, C.-L. Ping, L. Schirrmeister, G. Grosse, G. J. Michaelson, C. D. Koven,
450 J. A. O'Donnell, B. Elberling, U. Mishra, P. Camill, Z. Yu, J. Palmtag, P. Kuhry, Estimated stocks of circumpolar permafrost carbon with quantified uncertainty ranges and identified data gaps, Biogeosciences 11 (2014) 6573–6593.
- [5] J. Turner, J. E. Overland, J. E. Walsh, An arctic and antarctic perspective
455 on recent climate change, International Journal of Climatology 27 (2007) 277–293.
- [6] J. Hansen, R. Ruedy, J. Glascoe, M. Sato, Giss analysis of surface temperature change, Journal of Geophysical Research: Atmospheres 104 (1999) 30997–31022.

- 460 [7] A. C. I. Assessment, Impacts of a warming arctic-arctic climate impact assessment, Impacts of a Warming Arctic-Arctic Climate Impact Assessment, by Arctic Climate Impact Assessment, pp. 144. ISBN 0521617782. Cambridge, UK: Cambridge University Press, December 2004. 1 (2004).
- [8] C. D. Koven, B. Ringeval, P. Friedlingstein, P. Ciais, P. Cadule,
465 D. Khvorostyanov, G. Krinner, C. Tarnocai, Permafrost carbon-climate feedbacks accelerate global warming, Proceedings of the National Academy of Sciences 108 (2011) 14769–14774.
- [9] T. Osterkamp, Response of alaskan permafrost to climate, in: Fourth International Conference on Permafrost, Fairbanks, Alaska, 1983, pp. 17–
470 22.
- [10] M. A. Walvoord, R. G. Striegl, Increased groundwater to stream discharge from permafrost thawing in the yukon river basin: Potential impacts on lateral export of carbon and nitrogen, Geophysical Research Letters 34 (2007).
- 475 [11] S. Lyon, G. Destouni, R. Giesler, C. Humborg, C.-M. Mörtz, J. Seibert, J. Karlsson, P. Troch, Estimation of permafrost thawing rates in a sub-arctic catchment using recession flow analysis, Hydrology and Earth System Sciences 13 (2009) 595–604.
- [12] R. K. Pachauri, M. Allen, V. Barros, J. Broome, W. Cramer, R. Christ,
480 J. Church, L. Clarke, Q. Dahe, P. Dasgupta, et al., Climate change 2014: Synthesis report. contribution of working groups i, ii and iii to the fifth assessment report of the intergovernmental panel on climate change (2014).
- [13] C. D. Koven, W. J. Riley, A. Stern, Analysis of permafrost thermal dynamics and response to climate change in the CMIP5 earth system models,
485 Journal of Climate 26 (2013) 1877–1900.
- [14] S. Painter, J. Moulton, C. Wilson, Modeling challenges for predicting

hydrologic response to degrading permafrost, *Hydrogeology Journal* (2013) 1–4.

- 490 [15] B. L. Kurylyk, K. T. MacQuarrie, J. M. McKenzie, Climate change impacts on groundwater and soil temperatures in cold and temperate regions: Implications, mathematical theory, and emerging simulation tools, *Earth-Science Reviews* 138 (2014) 313–334.
- [16] R. Harlan, Analysis of coupled heat-fluid transport in partially frozen soil, *Water Resources Research* 9 (1973) 1314–1323.
- 495 [17] G. L. Guymon, J. N. Luthin, A coupled heat and moisture transport model for arctic soils, *Water Resources Research* 10 (1974) 995–1001.
- [18] G. S. Taylor, J. N. Luthin, A model for coupled heat and moisture transfer during soil freezing, *Canadian Geotechnical Journal* 15 (1978) 548–555.
- [19] K. Takata, S. Emori, T. Watanabe, Development of the minimal advanced treatments of surface interaction and runoff, *Global and planetary Change* 500 38 (2003) 209–222.
- [20] D. Nicolsky, V. Romanovsky, V. Alexeev, D. Lawrence, Improved modeling of permafrost dynamics in a gcm land-surface scheme, *Geophysical research letters* 34 (2007).
- 505 [21] D. M. Lawrence, A. G. Slater, S. C. Swenson, Simulation of present-day and future permafrost and seasonally frozen ground conditions in ccs4, *Journal of Climate* 25 (2012) 2207–2225.
- [22] J. M. McKenzie, C. I. Voss, D. I. Siegel, Groundwater flow with energy transport and water–ice phase change: numerical simulations, benchmarks, and application to freezing in peat bogs, *Advances in water resources* 510 30 (2007) 966–983.
- [23] V. Bense, G. Ferguson, H. Kooi, Evolution of shallow groundwater flow systems in areas of degrading permafrost, *Geophysical Research Letters* 36 (2009).

- 515 [24] S. L. Painter, S. Karra, Constitutive model for unfrozen water content in
subfreezing unsaturated soils, *Vadose Zone Journal* 13 (2014).
- [25] S. L. Painter, Three-phase numerical model of water migration in partially
frozen geological media: model formulation, validation, and applications,
Computational Geosciences 15 (2011) 69–85.
- 520 [26] R. E. Grimm, S. L. Painter, On the secular evolution of groundwater on
mars, *Geophysical Research Letters* 36 (2009) n/a–n/a. L24803.
- [27] A. Frampton, S. Painter, S. W. Lyon, G. Destouni, Non-isothermal, three-
phase simulations of near-surface flows in a model permafrost system under
seasonal variability and climate change, *Journal of Hydrology* 403 (2011)
525 352 – 359.
- [28] S. Karra, S. Painter, P. Lichtner, Three-phase numerical model for subsur-
face hydrology in permafrost-affected regions, *Cryosphere Discuss* 8 (2014)
149–185.
- [29] P. C. Lichtner, G. E. Hammond, C. Lu, S. Karra, G. Bisht, B. Andre, R. T.
530 Mills, J. Kumar, PFLOTRAN Web page, 2013. [Http://www.pflotran.org](http://www.pflotran.org).
- [30] J. Kumar, N. Collier, G. Bisht, R. T. Mills, P. E. Thornton, C. M.
Iversen, V. Romanovsky, Modeling the spatiotemporal variability in sub-
surface thermal regimes across a low-relief polygonal tundra landscape, *The*
Cryosphere 10 (2016) 2241–2274.
- 535 [31] S. L. Painter, E. T. Coon, A. L. Atchley, M. Berndt, R. Garimella, J. D.
Moulton, D. Svyatskiy, C. J. Wilson, Integrated surface/subsurface per-
mafrost thermal hydrology: Model formulation and proof-of-concept simu-
lations, *Water Resources Research* 52 (2016) 6062–6077.
- [32] E. T. Coon, J. D. Moulton, S. L. Painter, Managing complexity in simula-
540 tions of land surface and near-surface processes, *Water Resources Research*
78 (2016) 134–149.

- [33] M. Dall’Amico, S. Endrizzi, S. Gruber, R. Rigon, A robust and energy-conserving model of freezing variably-saturated soil, *The Cryosphere* 5 (2011) 469–484.
- 545 [34] M. F. Pikul, R. L. Street, I. Remson, A numerical model based on coupled one-dimensional richards and boussinesq equations, *Water Resources Research* 10 (1974) 295–302.
- [35] Y. Zhu, Y. Zha, J. Tong, J. Yang, Method of coupling 1-d unsaturated flow with 3-d saturated flow on large scale, *Water Science and Engineering* 4 (2011) 357–373.
- 550 [36] P. Hazenberg, Y. Fang, P. Broxton, D. Gochis, G.-Y. Niu, J. D. Pelletier, P. A. Troch, X. Zeng, A hybrid-3d hillslope hydrological model for use in earth system models, *Water Resources Research* 51 (2015) 8218–8239.
- [37] E. T. Coon, *ATS: The Advanced Terrestrial Simulator*, 2016.
- 555 <http://github.com/amanzi/ats>.
- [38] J. D. Moulton, M. Berndt, R. Garimella, L. Prichett-Sheats, G. Hammond, M. Day, J. Meza, High-level design of amanzi, the multi-process high performance computing simulator, office of environmental management, united states department of energy, washington dc (2012).
- 560 [39] M. Heroux, R. Bartlett, V. H. Hoekstra, J. Hu, T. Kolda, R. Lehoucq, K. Long, R. Pawlowski, E. Phipps, A. Salinger, H. Thornquist, R. Tuminaro, J. Wil-lenbring, A. Williams, An overview of trinos. Technical report sand2003-2927, Sandia National Laboratory (2003).
- [40] R. V. Garimella, W. A. Perkins, M. W. Buksas, M. Berndt, K. Lipnikov, E. Coon, J. D. Moulton, S. L. Painter, Mesh infrastructure for coupled multiprocess geophysical simulations, *Procedia Engineering* 82 (2014) 34 – 45.
- 565 [41] L. B. da Veiga, K. Lipnikov, G. Manzini, *The mimetic finite difference method for elliptic problems*, volume 11, Springer, 2014.

- [42] K. Lipnikov, G. Manzini, M. Shashkov, Mimetic finite difference method, *Journal of Computational Physics* 257 (2014) 1163–1227.
- [43] M. T. Calef, E. D. Fichtl, J. S. Warsa, M. Berndt, N. N. Carlson, Nonlinear krylov acceleration applied to a discrete ordinates formulation of the k-eigenvalue problem, *Journal of Computational Physics* 238 (2013) 188–209.
- [44] N. N. Carlson, K. Miller, Design and application of a gradient-weighted moving finite element code i: in one dimension, *SIAM Journal on Scientific Computing* 19 (1998) 728–765.
- [45] A. L. Atchley, S. L. Painter, D. R. Harp, E. T. Coon, C. J. Wilson, A. K. Liljedahl, V. E. Romanovsky, Using field observations to inform thermal hydrology models of permafrost dynamics with ats (v0.83), *Geoscientific Model Development* 8 (2015) 2701–2722.
- [46] A. L. Atchley, E. T. Coon, S. L. Painter, D. R. Harp, C. J. Wilson, Influences and interactions of inundation, peat, and snow on active layer thickness, *Geophysical Research Letters* 43 (2016) 5116–5123. 2016GL068550.
- [47] Lawrence Livermore National Laboratory, A mesh and field i/o library and scientific database, 2016. <https://wci.llnl.gov/simulation/computer-codes/silo>.
- [48] M. T. Jorgenson, Y. L. Shur, E. R. Pullman, Abrupt increase in permafrost degradation in arctic alaska, *Geophysical Research Letters* 33 (2006).
- [49] A. Liljedahl, L. Hinzman, J. Schulla, Ice-wedge polygon type controls low-gradient watershed-scale hydrology, in: *Proceedings of the Tenth International Conference on Permafrost*, volume 1, 2012, pp. 231–236.
- [50] L. D. Hinzman, N. D. Bettez, W. R. Bolton, F. S. Chapin, M. B. Dyurgerov, C. L. Fastie, B. Griffith, R. D. Hollister, A. Hope, H. P. Huntington, et al., Evidence and implications of recent climate change in northern alaska and other arctic regions, *Climatic Change* 72 (2005) 251–298.

- [51] J. C. Rowland, C. E. Jones, G. Altmann, R. Bryan, B. T. Crosby, L. D. Hinzman, D. L. Kane, D. M. Lawrence, A. Mancino, P. Marsh, J. P. McNamara, V. E. Romanovsky, H. Toniolo, B. J. Travis, E. Trochim, C. J. Wilson, G. L. Geernaert, Arctic landscapes in transition: Responses to thawing permafrost, *Eos, Transactions American Geophysical Union* 91 (2010) 229–230.